Applied Mathematics and Computation 213 (2009) 47–59

Contents lists available at ScienceDirect

Applied Mathematics and Computation

journal homepage: www.elsevier.com/locate/amc

Central unstaggered finite volume schemes for hyperbolic systems: Applications to unsteady shallow water equations

R. Touma

Computer Science and Mathematics, Lebanese American University, Beirut, Lebanon

ARTICLE INFO

Keywords:
Unstaggered central schemes
Shallow water equations
Source terms
Non-oscillatory
Limiters
Finite volume methods

ABSTRACT

A class of central unstaggered finite volume methods for approximating solutions of hyperbolic systems of conservation laws is developed in this paper. The proposed method is an extension of the central, non-oscillatory, finite volume method of Nessyahu and Tadmor (NT). In contrast with the original NT scheme, the method we develop evolves the numerical solution on a single grid; however ghost cells are implicitly used to avoid the resolution of the Riemann problems arising at the cell interfaces. We apply our method and solve classical one and two-dimensional unsteady shallow water problems. Our numerical results compare very well with those obtained using the original NT method, and are in good agreement with corresponding results appearing in the recent literature, thus confirming the efficiency and the potential of the proposed method.

1. Introduction

In the early nineties, Nessyahu and Tadmor [21] presented a non-oscillatory central scheme for the numerical resolution of hyperbolic systems of conservation laws. The NT scheme is based on the staggered Lax–Friedrichs method; It avoids the resolution of the Riemann problems arising at the cell interfaces by evolving the numerical solution on an original grid and on a staggered dual one at consecutive time steps. The NT scheme is second-order accurate thanks to a piecewise linear numerical solution defined on the computational cells; Furthermore the NT scheme uses slope-limiting to guarantee oscillation-free numerical solutions.

Multidimensional extensions of the NT scheme on Cartesian grids (squares or cubes) [3,18] or unstructured grids (triangles or tetrahedrons) [2,5] have been proposed for solving hyperbolic systems. These multidimensional extensions were intensively and successfully used to solve problems arising in aerodynamics [3–5], astrophysics and magnetohydrodynamics [6,27], and others.

However, the fact that the numerical solution, in the NT-type schemes, alternates between two grids at successive time steps is considered as a weakness of the method. More precisely, if the numerical solution obtained using an NT-type base scheme requires additional treatment in order to satisfy a physical property, a synchronization problem arises since any treatment of the updated solution involves the solution values computed at different previous times. The situation becomes even harder when the original and the dual staggered cells are not of the same shape. This problem was observed in a previous work when we used central schemes to solve magnetohydrodynamic "MHD" problems in two and three space dimensions. We recall that when solving ideal MHD problems, the accumulation of numerical errors such as the truncation or round-off errors can usually lead to a non-physical phenomenon known as magnetic monopoles, i.e., when the magnetic field **B** in the numerical solution is not solenoidal. As a consequence, negative pressures and densities and other non-physical waves can arise [9]. To satisfy the physical requirement, several methods were developed but none of them (including the Constrained Transport

E-mail address: rony.touma@lau.edu.lb

0096-3003/$ - see front matter © 2009 Elsevier Inc. All rights reserved.
doi:10.1016/j.amc.2009.02.059

method) was directly applicable along with central schemes. So we had to develop a special *Constrained Transport*-type method that is applicable with central schemes to treat the magnetic field components in the numerical solution on both the original and staggered cells [6,27].

The same problem arises when we use central schemes to solve shallow magnetohydrodynamic "SMHD" problems. A similar problem is encountered when central schemes are used to solve shallow water problems on variable bottom topography. This problem will be clearly described in a later section of this paper.

Shallow water equations (SWE) represent a good mathematical model for the hydrodynamics of coastal oceans, simulation of flows in channels and rivers, study of large-scale waves and vertically averaged regimes in the atmosphere and ocean. In the case of a flat bottom topography, the shallow water system is a hyperbolic system. A source term is added to the right-hand side of the hyperbolic system when the bottom topography is variable.

Several numerical methods were developed to solve shallow water problems with variable bottom topography: Well-balanced schemes were constructed in [7,16]; Schemes based on the solution of the non-homogeneous Riemann-problem were proposed in [16,15]. We also cite the finite difference "Roe schemes" of Gallouët et al. [13], and the central upwind schemes of Kurganov and Levy [19]. Higher order schemes for nonlinear conservation laws with exact or approximate Riemann solvers and local characteristic decomposition were presented in [1,22,23].

To solve SWE problems with variable bottom topography, two approaches are possible: The first one consists of rewriting the SWE system with source term in a non conservative form by introducing an additional equation. The result is a system without source term and is known as the augmented system. A disadvantage of this approach is that it generates non-physical waves such as negative water heights in the case of wet/dry fronts [10].

The second approach deals with the complete SWE system (i.e. the hyperbolic system and the source term); it consists of using Strang's [24] fractional-step splitting method by first solving the hyperbolic system with the numerical base scheme, and then applying a quadrature formula to integrate the source term.

For the NT-type central schemes which rest on the use of an original and a dual staggered grid, direct use of the fractional-step method is not immediate since any quadrature formula considered to treat the source term requires solution values and the bottom topography function's gradient obtained on both the original grid and the staggered dual one. Eventually a synchronization problem arises and additional staggering of the solution's components is necessary, and the bottom topography's gradient needs to be defined on both grids.

In 1998, Jiang et al. [17] presented a first unstaggered adaptation of the NT scheme; the method they proposed utilizes both iteration formulas of Nessyahu and Tadmor, but with a zero time-step for the second iteration.

In a previous work [28] we have developed a one-dimensional unstaggered central scheme for hyperbolic systems. The method we presented in [28] can be viewed as an unstaggered adaptation of the NT scheme, and a generalization of the method presented by Jiang et al. [17].

In this paper we develop a class of second-order accurate unstaggered central schemes ("UCS") to solve general one and two-dimensional hyperbolic systems of conservation laws and in particular to solve unsteady shallow water problems. The method we propose is a one-parameter method in one space dimension; two parameters are involved in two-dimensional space. The base scheme evolves the numerical solution on a single grid, but it uses ghost staggered cells to avoid the resolution of the Riemann problems arising at the cell interfaces. Strang's fractional-step method shall be used to treat the source term in the case of variable bottom topographies. The resulting scheme is an easy-to-implement, second-order accurate, non-oscillatory, unstaggered central scheme.

The method developed here is then used to solve some classical one and two-dimensional SWE problems; the numerical results obtained in Section 4 are in good agreement with corresponding ones appearing in the recent literature, and thus confirm the efficiency and potential of the proposed method.

2. Shallow water equations

The Saint–Venant equations, also known as the shallow water equations, describe the motion of an inviscid and incompressible fluid under gravity, over a variable bottom topography, with a free surface. Recently, the shallow water equations have been used to model the propagation of tsunamis and inundations, river floods, dam breaches, and other problems. Written in their conservation form, the shallow water equations are:

$$\frac{\partial}{\partial t}\begin{pmatrix} h \\ hu \\ hv \end{pmatrix} + \frac{\partial}{\partial x}\begin{pmatrix} hu \\ hu^2 + \frac{1}{2}gh^2 \\ huv \end{pmatrix} + \frac{\partial}{\partial y}\begin{pmatrix} hv \\ huv \\ hv^2 + \frac{1}{2}gh^2 \end{pmatrix} = \begin{pmatrix} 0 \\ -gh\frac{\partial b}{\partial x} \\ -gh\frac{\partial b}{\partial y} \end{pmatrix}. \tag{1}$$

Here $h(x,y,t)$ denotes the fluid height, $u(x,y,t)$ and $v(x,y,t)$ are the velocity components in the x and y-directions, respectively; g is the gravitational constant. The bottom elevation function is $z = b(x,y)$ (see Fig. 1).

In the case of a flat bottom topography, the source term in system (1) vanishes, and we obtain a hyperbolic system of three conservation laws with real eigenvalues and a complete set of linearly independent eigenvectors. Detailed study of the hyperbolic structure of the system is found in [14].

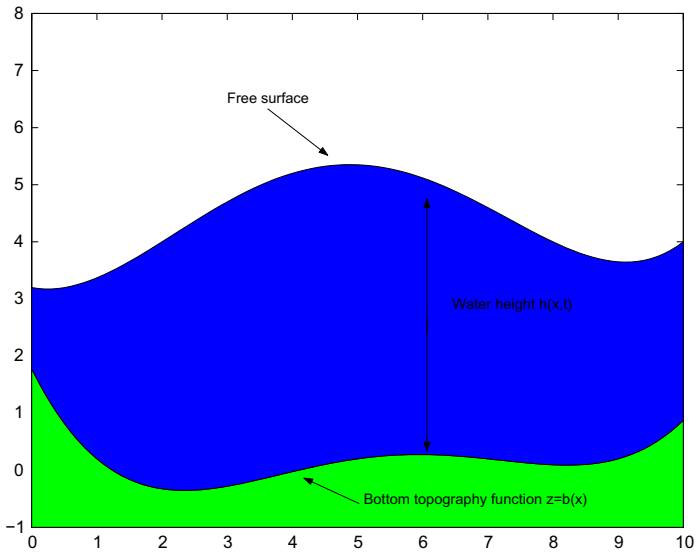

Fig. 1. Water flow over a variable topography.

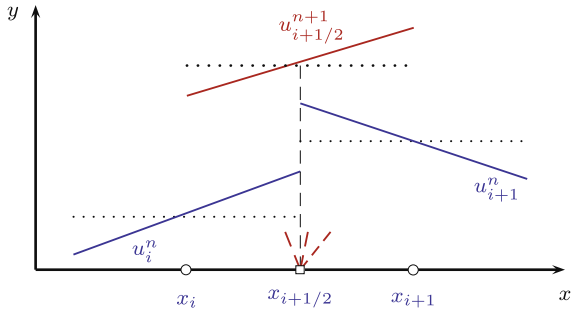

Fig. 2. The resolution of Riemann problems at cell interfaces is avoided when alternating from original to staggered grid.

3. Numerical scheme

In this section we develop a family of central unstaggered numerical schemes for solving general hyperbolic systems and in particular SWE problems. First we present a brief review of the Lax–Friedrichs/Nessyahu–Tadmor scheme, and then the UCS method (unstaggered central scheme) is developed in one and two space dimensions.

3.1. One-dimensional Nessyahu–Tadmor central scheme

We consider the initial value problem:

$$\begin{cases} u_t + f(u)_x = 0, \\ u(x, t = 0) = u_0(x). \end{cases} \tag{2}$$

The NT scheme [21] is based on the staggered Lax-Friedrichs method: It avoids the resolution of the Riemann problems at the cell interfaces by alternating the numerical solution on an original and a staggered grid. Furthermore the NT scheme uses a piecewise linear reconstruction of the piecewise constant solution obtained at the previous time-step (see Fig. 2):

$$u(x, t^n) = L_i(x, t^n) = u_i^n + (x - x_i)\frac{(u_i^n)'}{\Delta x}, \tag{3}$$

where

$$\frac{(u_i^n)'}{\Delta x} \cong \frac{\partial}{\partial x} u(x, t^n)|_{x=x_i} + \mathcal{O}(\Delta x)$$

approximates the slope to first-order accuracy; this leads to a numerical solution accurate to the second-order in space. Second-order temporal accuracy is guaranteed thanks to a predictor–corrector time discretization. The solution at time t^{n+1} is computed on the staggered cells using the formula:

$$u_{i+1/2}^{n+1} = \frac{1}{2}\left(u_{i+1}^{n} + u_{i}^{n}\right) + \frac{1}{8}\left(\left(u_{i}^{n}\right)' - \left(u_{i+1}^{n}\right)'\right) - \frac{\Delta t}{\Delta x}\left(f\left(u_{i+1}^{n+1/2}\right) - f\left(u_{i}^{n+1/2}\right)\right). \tag{4}$$

The values at the intermediate time $t^{n+1/2}$ are defined by Eq. (6) below. The solution on the original grid will be computed at time t^{n+2} using a similar formula. For a complete description of the one-dimensional NT scheme, one is referred to [21]. Multidimensional extensions of the NT scheme on Cartesian or unstructured grids can be found in [2–4,18,27].

3.2. One-dimensional unstaggered central schemes

We now extend the Nessyahu–Tadmor scheme and construct our unstaggered central scheme while preserving all properties of the original NT scheme. The method we develop computes the numerical solution on a single grid but uses "ghost" staggered cells to avoid the resolution of the Riemann problems at the cell interfaces when updating the numerical solution. Piecewise linear reconstructions of the numerical solution defined at the center of the ghost cells send back the updated solution to the original grid. We assume that the computational domain, say the interval $[a,b]$, is discretized using the nodes x_i, centers of the cells $C_i = \left[x_{i-1/2}, x_{i+1/2}\right]$ of length Δx, and we assume that the numerical solution is given at time t^n at the nodes x_i (i.e. we assume that $\{u_i^n\}_i$ is known). The solution at a later time t^{n+1} is computed in two steps as follows:

In the first step, we define the ghost staggered cells $G_{i+1/2} = [x_i, x_{i+1}]$ and obtain an estimate $u_{i+1/2}^G$ of the solution at time t^{n+1} on the ghost cells $G_{i+1/2}$ using Nessyahu and Tadmor's formula (4) as follows:

$$u_{i+1/2}^{G} = \frac{1}{2}\left(u_{i+1}^{n} + u_{i}^{n}\right) + \frac{1}{8}\left(\left(u_{i}^{n}\right)' - \left(u_{i+1}^{n}\right)'\right) - \lambda\left(f\left(u_{i+1}^{n+1/2}\right) - f\left(u_{i}^{n+1/2}\right)\right), \tag{5}$$

where $\lambda = \frac{\Delta t}{\Delta x}$. Solving the Riemann problems arising at the points $x_{i+1/2}$ in Eq. (5) is by-passed thanks to the staggered ghost cells. Values $u_i^{n+1/2}$ at the intermediate time $t^{n+1/2}$ in Eq. (5) are approximate values defined by an intermediate predictor step using a first-order Taylor expansion and the original system (2) as follows:

$$u\left(x_i, t^{n+1/2}\right) \cong u(x_i, t^n) + \frac{\Delta t}{2} u_t(x_i, t^n) \cong u_i^n - \frac{\Delta t}{2} f(u)_x|_{(x_i, t^n)} \cong u_i^n - \frac{\Delta t}{2\Delta x} f_i' \equiv u_i^{n+1/2}, \tag{6}$$

where $f_i'/\Delta x$ is an approximate flux derivative. The numerical derivatives $\left\{\left(u_i^n\right)'\right\}$ in Eq. (4) and the flux derivatives $\{(f_i)'\}$ in Eq. (6) are carefully computed with limiters to avoid spurious oscillations in the numerical solution [21].

In this work we have mainly used van Leer's monotonized centered limiter ($MC-\theta$) [29], where the slope of the reconstruction, in the one-dimensional case, is chosen as

$$\left(u_i^n\right)' = \operatorname{minmod}\left[\left(\theta\left(u_i^n - u_{i-1}^n\right), \frac{u_{i+1}^n - u_{i-1}^n}{2}, \theta\left(u_{i+1}^n - u_i^n\right)\right)\right], \tag{7}$$

and where θ is chosen such that $1 \leqslant \theta \leqslant 2$.

One may also use the minmod limiter defined below, but as we shall see in Section 4, better results are obtained with the $MC-\theta$ limiter.

$$\left(u_i^n\right)' = \operatorname{minmod}\left(\frac{u_i - u_{i-1}}{\Delta x}, \frac{u_{i+1} - u_i}{\Delta x}\right), \tag{8}$$

where minmod is defined as

$$\operatorname{minmod}(a,b) = \begin{cases} \operatorname{sgn}(a) \cdot \min\{|a|, |b|\}, & \text{if } a \cdot b > 0, \\ 0 & \text{otherwise.} \end{cases} \tag{9}$$

Other limiters may also be used to estimate the numerical derivatives [25].

The second step of the proposed UCS method consists in sending the updated solution obtained on the ghost staggered cells back to the original grid. Since the numerical solution is defined using piecewise linear reconstructions of the piecewise constant solution defined at the center of the cells C_i and $G_{i+1/2}$, we first define the piecewise linear reconstructions of the ghost cell values $u_{i-1/2}^G$:

$$u_{i-1/2}^{G}\left(x, t^{n+1}\right) = u_{i-1/2}^{G} + \left(x - x_{i-1/2}\right)\frac{\left(u_{i-1/2}^{G}\right)'}{\Delta x}, \tag{10}$$

with $0 < |x - x_{i-1/2}| < \Delta x/2$ and where $\left(u_{i-1/2}^G\right)'/\Delta x$ is an approximate slope associated with the piecewise linear interpolant in the ghost cell $G_{i-1/2}$; we then define the solution values u_i^{n+1} (Fig. 3) at the center of the cell $\left[x_{i-1/2}, x_{i+1/2}\right]$ using the formula:

$$u_i^{n+1} = \frac{1}{2}\left(u_{i-1/2}^{G}\left(x_{i-1/2} + \alpha\Delta x, t^{n+1}\right) + u_{i+1/2}^{G}\left(x_{i+1/2} - \alpha\Delta x, t^{n+1}\right)\right). \tag{11}$$

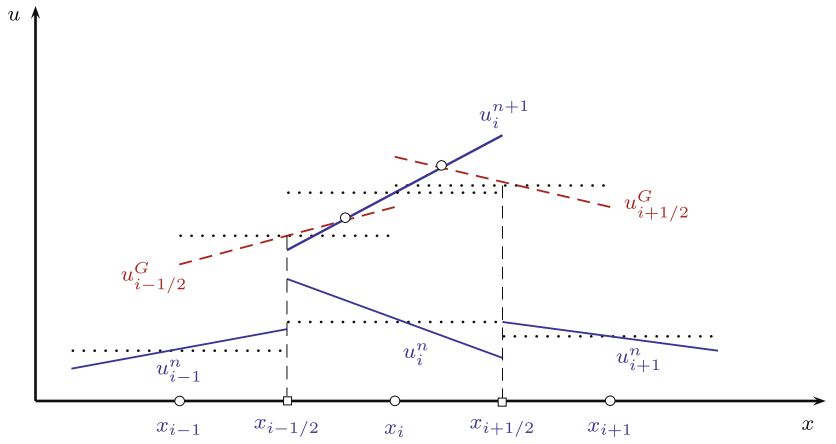

Fig. 3. The resolution of Riemann problems at cell interfaces is avoided when alternating from original to staggered grid.

The values of the parameter α in Eq. (11) range between 0 and 1/2; however as we shall see in Section 4, best results are obtained when $\alpha = 1/4$ and the resulting scheme is second-order accurate both in space and time, since for $\alpha = 1/4$, Eq. (11) is rewritten using first-order Taylor expansions with respect to x as

$$u_i^{n+1} = \frac{1}{2}\left(u_{i-1/2}^G + u_{i+1/2}^G\right) + \frac{1}{8}\left(\left(u_{i-1/2}^G\right)' - \left(u_{i+1/2}^G\right)'\right). \tag{12}$$

The right-hand-side of Eq. (12) stands for the second equation of the original Nessyahu and Tadmor scheme [21] but obtained with a dummy time-step $\Delta t = 0$. To summarize, the algorithm of the proposed one-dimensional unstaggered central scheme proceeds as follows: Knowing the solution at time t^n, we update the solution on the ghost cells using Eq. (5) and then we obtain the solution at time t^{n+1} on the original and unique grid using Eq. (11). The proposed UCS scheme possesses the same stability condition as the original NT; furthermore, for $\alpha = 1/4$, the method we obtain is the same as that proposed in [17].

3.3. Two-dimensional unstaggered central schemes

In 1995, Arminjon et al. [2,3] presented finite volume extensions of the Nessyahu–Tadmor scheme to unstructured triangular [2] or Cartesian rectangular [3] two-dimensional grids. The schemes they presented evolve a numerical solution on an original grid and a staggered dual one, thus avoiding the time-consuming process of resolving the Riemann problems that arise at the cell interfaces. In [3], the cells of both the original and dual staggered grids are Cartesian. Fig. 4 shows four cells ($C_{i,j}$, $C_{i+1,j}$, $C_{i,j+1}$, and $C_{i+1,j+1}$) of the original grid and the dual cell $D_{i+1/2,j+1/2}$ of the staggered grid. Given the numerical solution u_{ij}^n at time t^n on the original grid, the solution at time t^{n+1} on the staggered grid is computed using the formula:

$$\begin{aligned} u_{i+1/2,j+1/2}^{n+1} = {} & \frac{1}{4}\left(u_{ij}^n + u_{i+1,j}^n + u_{i,j+1}^n + u_{i+1,j+1}^n\right) + \frac{1}{16}\left(u_{i,j;x}^{lim} - u_{i+1,j;x}^{lim}\right) - \frac{\lambda}{2}\left[f_{i+1,j}^{n+1/2} - f_{ij}^{n+1/2}\right] + \frac{1}{16}\left(u_{ij+1;x}^{lim} - u_{i+1,j+1;x}^{lim}\right) \\ & - \frac{\lambda}{2}\left[f_{i+1,j+1}^{n+1/2} - f_{i,j+1}^{n+1/2}\right] + \frac{1}{16}\left(u_{i,j;y}^{lim} - u_{ij+1;x}^{lim}\right) - \frac{\lambda}{2}\left[g_{ij+1}^{n+1/2} - g_{ij}^{n+1/2}\right] + \frac{1}{16}\left(u_{i+1,j;y}^{lim} - u_{i+1,j+1;x}^{lim}\right) \\ & - \frac{\lambda}{2}\left[g_{i+1,j+1}^{n+1/2} - g_{i+1,j}^{n+1/2}\right], \end{aligned} \tag{13}$$

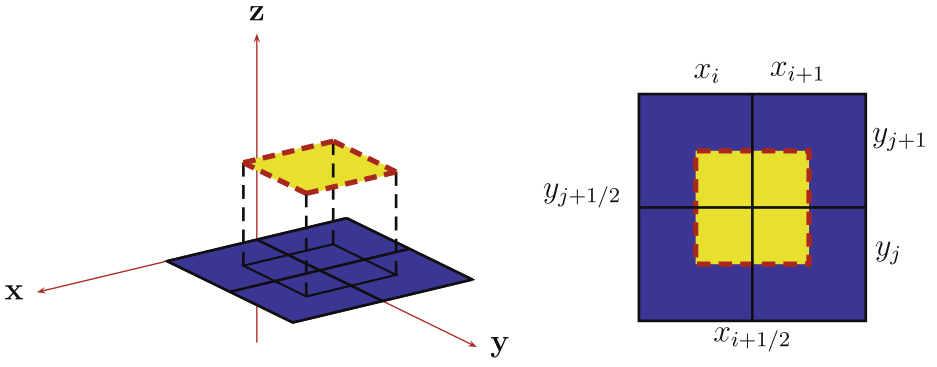

Fig. 4. (Left) Four original cells for the solution at time t^n and a staggered dual cell for the solution at time t^{n+1}.

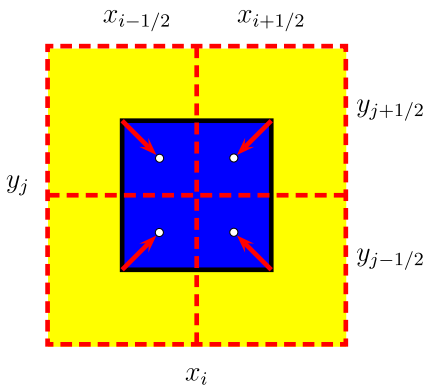

Fig. 5. Four ghost cells (dashed line boundaries) are necessary to define the solution on the original Cartesian cell C_{ij} (solid line boundary).

where $\lambda = \Delta t/\Delta x$, and $(\nabla u) \equiv \left(u_x^{lim}/\Delta x + \mathcal{O}(\Delta x), u_y^{lim}/\Delta y + \mathcal{O}(\Delta y)\right)$ is a limited gradient of the numerical solution. The components of the gradient vector are estimated using either the $MC-\theta$ or the minmod limiter separately for the x component and the y component, respectively.

A similar formula computes the numerical solution on the cells of the original grid at time t^{n+2}. A detailed description of Arminjon's two-dimensional extension of the NT scheme is found in [3,18].

The two-dimensional version of the UCS method evolves a piecewise linear numerical solution on a unique grid discretized using the nodes x_{ij} centers of the cells $C_{ij} = \left[x_{i-1/2}, x_{i+1/2}\right] \times \left[y_{j-1/2}, y_{j+1/2}\right]$. As in the one-dimensional case if the solution u_{ij}^n is known at time t^n, we obtain the solution at the following time $t^{n+1} = t^n + \Delta t$ in two steps: First we obtain an update of the solution on the ghost cells $G_{i+1/2,j+1/2} = [x_i, x_{i+1}] \times [y_j, y_{j+1}]$ using the first Eq. (13) of the two-dimensional central scheme to by-pass the resolution of the Riemann problems at the cell interfaces. The solution at the center of the cell C_{ij} is then obtained using piecewise linear reconstructions of the piecewise constant solution defined at the center of the cells $G_{i+1/2,j+1/2}$ (Fig. 5) according to the formula:

$$u_{ij}^{n+1} = \frac{1}{4}\left(u^G_{i-1/2+\alpha,j-1/2+\beta} + u^G_{i+1/2-\alpha,j-1/2+\beta} + u^G_{i+1/2-\alpha,j+1/2-\beta} + u^G_{i-1/2+\alpha,j+1/2-\beta}\right), \tag{14}$$

where the interpolated values in Eq. (14) are obtained as follows:

$$u^G_{i-1/2+\alpha,j-1/2+\beta} = u^G_{i-1/2,j-1/2} + \alpha \overrightarrow{U}^{G,lim}_{i-1/2,j-1/2;x} + \beta \overrightarrow{U}^{G,lim}_{i-1/2,j-1/2;y}. \tag{15}$$

Again $\left(\nabla \overrightarrow{U}^G\right) \equiv \left(\overrightarrow{U}_x^{G,lim}/\Delta x + \mathcal{O}(\Delta x), \overrightarrow{U}_y^{G,lim}/\Delta y + \mathcal{O}(\Delta y)\right)$ is a limited gradient of the numerical solution calculated on the ghost cells. As in the one-dimensional case, the parameters α and β used in the linear reconstructions range between 0 and 1/2. Setting $\alpha = \beta = 1/4$ yields second-order accuracy in space. The resulting two-dimensional UCS method shares the same stability condition as the two-dimensional central scheme presented in [3,18].

3.4. Numerical treatment of the source term

Variable bottom topography in the case of shallow water problems results in a nonzero source term in Eq. (1); the resulting mathematical model cannot be exactly solved. The numerical scheme developed in the previous section is applicable when we are solving homogeneous hyperbolic conservation laws. To solve general SWE problems we apply Strang's fractional-step method [24] which summarizes as follows. To numerically solve a non-homogeneous system of the form

$$q_t + f(q)_x = \psi(q, x),$$

we first solve the conservation law

$$q_t + f(q)_x = 0,$$

using the numerical base scheme, and then we integrate the ordinary differential equation

$$q_t = \psi(q, x),$$

using a midpoint-type second-order Runge–Kutta formula. If we denote by q_h the numerical approximation of the solution at time t^{n+1} obtained using the base scheme, then the solution of the (SWE) problem at time t^{n+1} is obtained using the following two-step procedure:

$$q^* = q_h + \frac{\Delta t}{2}\psi(q_h, x),$$

followed by

$$q^{n+1} = q_h + \Delta t \psi(q^*, x).$$

Here we emphasize the fact that this Runge–Kutta formula conserves the second-order accuracy of the numerical base scheme.

A similar treatment of the source term is performed in the case of two-dimensional SWE problems.

4. Numerical experiments

In this section we apply our unstaggered central scheme and solve classical one and two-dimensional SWE problems in the case of flat/variable bottom topography. To validate our method we compare some of the numerical results obtained using the UCS method with those obtained using the original Nessyahu–Tadmor scheme. Let us mention here that when we use the original NT scheme to solve SWE problems with variable bottom topographies, and in order to treat the resulting source term, we need to discretize the bottom topography function on both the original and the staggered grids; furthermore, additional staggering of the numerical solution components is also required.

The fact that central schemes evolve the numerical solution on an original and a staggered grid to avoid the resolution of the Riemann problems at the cell interfaces represents a restriction on the computation of the time-step as compared to other numerical methods. As described in [21] for the 1D case, and later in [3–5,18] for the multidimensional central schemes, the CFL number for central schemes is about 0.5. Even with this time-step restriction, experience has shown that the computing times of central schemes are often substantially shorter than those of methods based on exact or approximate Riemann solvers [4]. The numerical results we present later in this section are obtained using a CFL number of 0.475. It is also known that, in the case of central schemes as well as other numerical methods, the choice of the limiter in the numerical computation of gradients may contribute in a significant way to the quality of the numerical resolution. Before considering SWE problems, we first validate the numerical base scheme by considering the simple scalar advection problem $u_t + u_x = 0$ with the initial condition $u_0(x) = 4$ inside the interval $|x - 0.5| \leqslant 0.15$ and $u_0(x) = 1$ elsewhere in the computational domain $[0, 1]$. The analytic solution for this initial value problem is given at all time t in terms of the initial condition as $u(x, t) = u_0(x - t)$. We apply the UCS method and compute the numerical solution at time $t = 0.05$ and compare it to the exact solution.

Fig. 6 shows the numerical solution obtained using 100 grid points with different values of α. A good agreement between the numerical/exact solution is observed in this gra

4.1. Test case 1: vacuum over discontinuous topography

For our first numerical experiment, we consider the *vacuum over discontinuous topography* problem as considered in [8,13]. The problem features a strong double rarefaction which leads to developing cavitation over variable topography. The computational domain is the interval $[0, 25]$ of the x-axis discretized with 2000 gridpoints; the solution is computed at the final time $t = 0.25$. The bottom's topography function $b(x)$ and the initial condition $u(x)$ are defined as follows:

$$b(x) = \begin{cases} 1 & \text{if } 25/3 < x < 12.5, \\ 0 & \text{otherwise.} \end{cases} \quad \text{and} \quad u(x, 0) = \begin{cases} -35 & \text{if } x < 50/3, \\ 35 & \text{otherwise.} \end{cases} \tag{16}$$

The initial water height for this problem is $h(x, 0) = 10$. Fig. 7 shows the water height h (left), and the momentum hu (right) at the final time; the dotted curve is obtained using the original NT scheme with the appropriate original and staggered

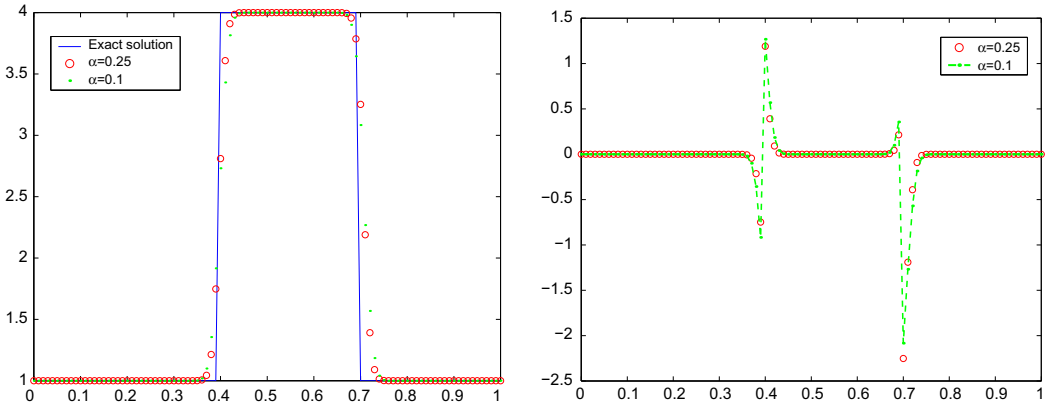

Fig. 6. Scalar advection test: (Left) The exact solution is shown in solid line, solutions obtained using $\alpha = 0.25$ and $\alpha = 0.1$ are shown in "o" and "·", respectively. (Right) Plot of the error between the exact and the numerical solution obtained using $\alpha = 0.25$ ("o") and $\alpha = 0.1$ (dashed line).

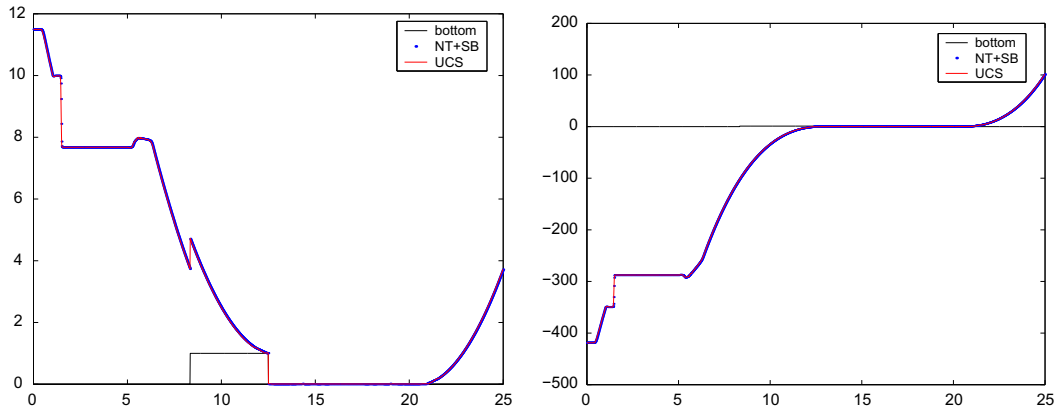

Fig. 7. Test case 1: Total water height at the final time (left) and the momentum (right). The dotted curve in both graphs is obtained using the original NT scheme with the appropriate staggered bottom (SB) topography function at each time-step. The solid line is obtained using the new UCS scheme on a single grid with one bottom topography function.

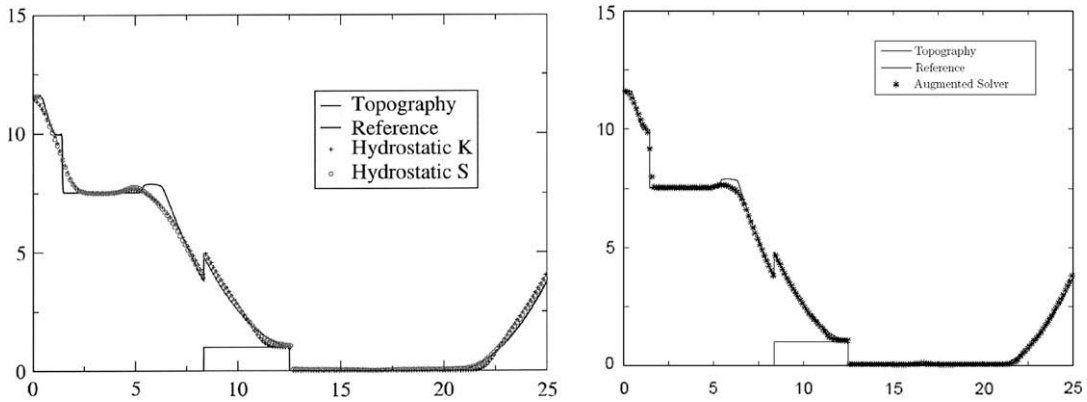

Fig. 8. Solution of the "vacuum over discontinuous topography" problem obtained using: (left) positive preserving methods near a dry front and, (right) augmented system and the wave propagation method as presented in [14].

bottom topography (SB) functions at each time-step, while the solid line is obtained using the new unstaggered scheme computed on a single grid. Results obtained using both schemes are indistinguishable and are in perfect agreement with those appearing in [8,13]. Fig. 8 is borrowed from [14]; on the left we see solutions obtained using several positivity preserving methods near a dry front; the reference solution is obtained using the wave propagation method. As described by Bouchut in [8], the water height is systematically underestimated on the front when such methods are applied. This fact is improved when the augmented system is used as is observed in Fig. 8(right). Fig. 7 shows that the water height doesn't flatten at the dry front as compared to the results shown in Fig. 8.

4.2. Test case 2: water flow over variable bottom topography

For our second experiment we consider another classical problem previously considered in [20]. The computational domain is the interval $[-10, 10]$ of the x-axis, and is discretized using 2000 gridpoints. The bottom topography is given by the function $b(x) = b_c\left(1 - \frac{x^2}{4}\right)$ if $-2 \leqslant x \leqslant 2$ and $b(x) = 0$ otherwise. The initial conditions are $h(x,0) = 1 - b(x)$ for the initial water height and $u(x,0) = u_0$ is the initial velocity. Free boundary conditions are applied. The numerical solution is computed at time $t = 20$. In this problem we used $b_c = 0.2$, $u_0 = 1$, and $g = 1$ (the gravitational constant). We have solved this problem using our unstaggered central scheme with $\alpha = 1/4$ and using the original Nessyahu–Tadmor scheme. For the latter case the bottom topography function was defined on the staggered grid in order to treat the source term at odd time steps. Fig. 9 shows a comparison between the numerical results obtained using both numerical schemes. Fig. 10 shows the difference between the results for the water height obtained at the final time using the UCS and the NT methods on 2000 gridpoints. The numerical results obtained using both schemes are undistinguishable and are in very good agreement with corresponding results appearing in the literature, thus confirming the efficiency and the potential of our proposed unstaggered central scheme.

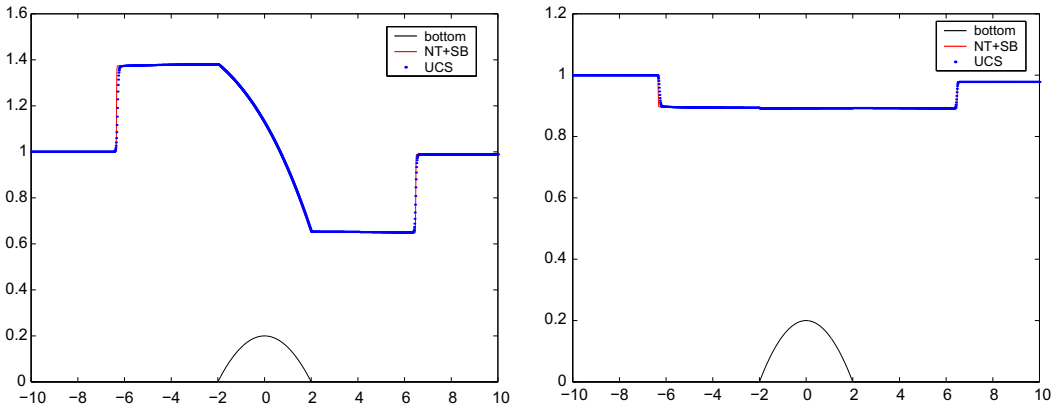

Fig. 9. Test case 2: Total water height at the final time (left) and the momentum (right).

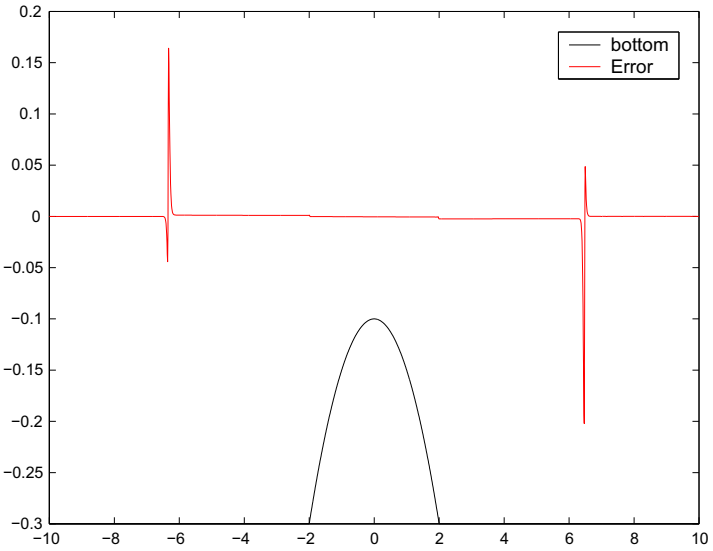

Fig. 10. Test case 2: Error between the results for the water height obtained using the UCS/NT methods on 2000 gridpoints.

4.3. Two-dimensional flow over variable bottom topography

Our first two-dimensional experiment is an extension of the one-dimensional water flow problem over a variable bottom topography [20]. The computational domain is the square $[-10,10]^2$ of the xy-plane, discretized using 200^2 gridpoints. The bottom topography function over the computational domain is given by $b(x,y) = b_c\left(1-\frac{x^2}{4}\right)$ if $-2 \leqslant x \leqslant 2$ and $b(x,y) = 0$ elsewhere. The initial water height and velocity field are $h(x,y) = 1 - b(x,y)$ and $(u,v) = (1,0)$, respectively. Fig. 11(left) shows the water height at time $t = 20$ s. Fig. 11(right) shows a plot (dotted curve) of the water height along the line $y = 0$ at the final time. The reference solution (solid line) is the solution of the corresponding one-dimensional problem computed on 2000 gridpoints. A good agreement between both curves is observed in this figure.

4.4. Two-dimensional circular dam-break problem

Our second two-dimensional experiment is the circular dam-break problem previously considered in [12] and originally presented in [1]. The experiment consists of breaking a circular dam of radius 11 m, centered at the point (25,25) of the square $[0,50]^2$. The water height inside the circular dam is $h = 10$ m and 1 m outside. Initially the water is at rest all over the domain ($u = v = 0$). The cylindrical wall is suddenly removed and the water will spread and propagate radially and symmetrically, and a transition from subcritical to supercritical flow will take place.

The computational domain is discretized using 200^2 gridpoints and the numerical solution is computed at the final time $t = 0.69$ s with the $MC - \theta = 2$ limiter.

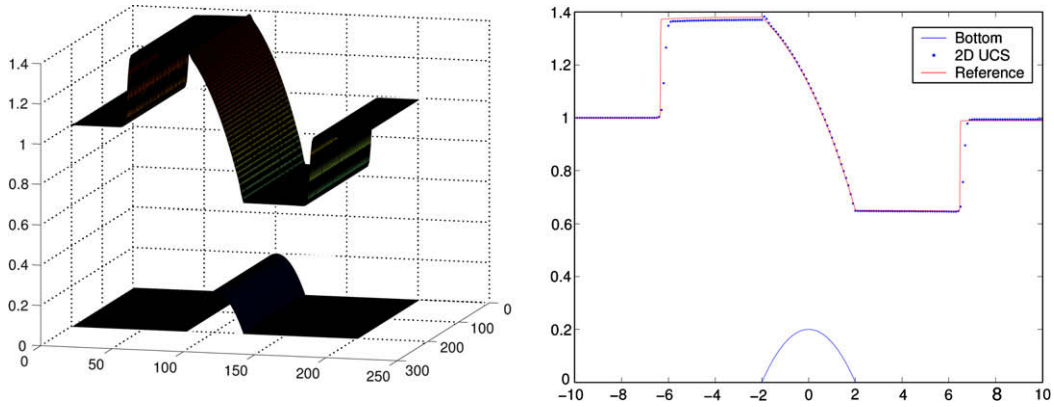

Fig. 11. Test case 2: Total water height (left) and water height along the line $y = 0$ (right), at the final time.

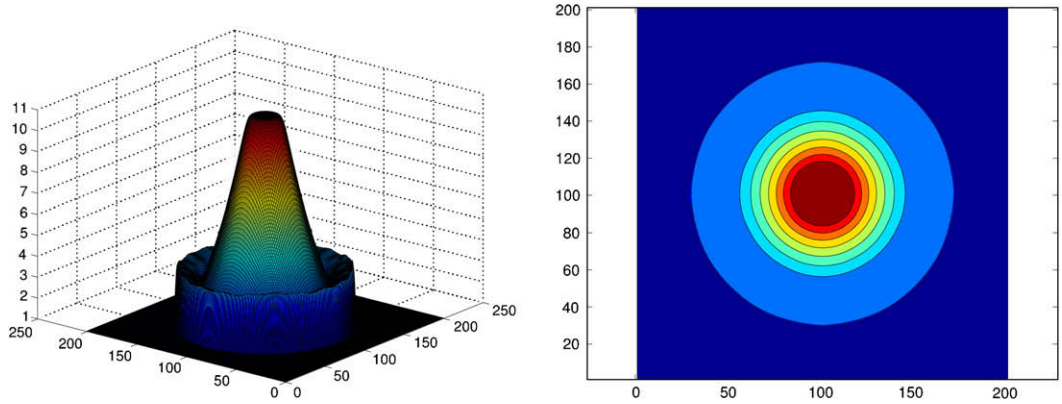

Fig. 12. Two-dimensional circular dam-break problem: water height (left) and contour lines of the water height (right) at the final time $t = 0.69$.

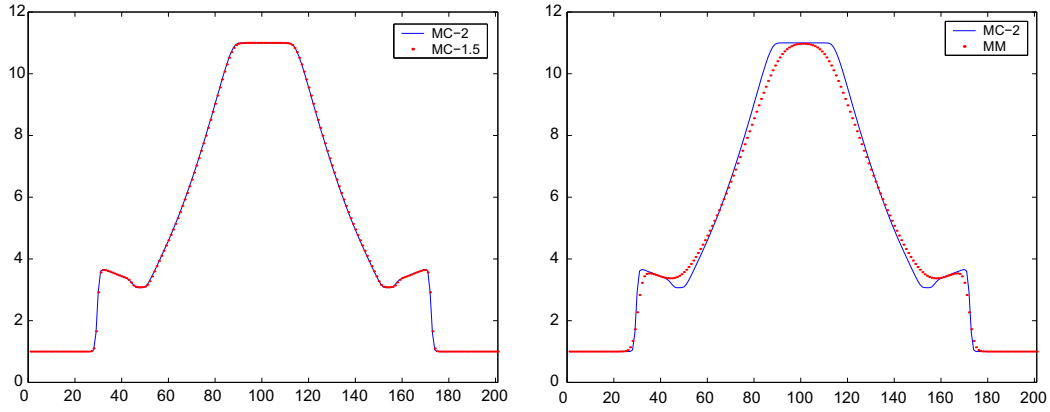

Fig. 13. Two-dimensional circular dam-break problem: Water height at the final time obtained using the $MC-2$ vs. $MC-1.5$ limiter (left) and the $MC-2$ vs. MinMod limiter (right).

Fig. 12(left) shows the water height h at the final time, and Fig. 12(right) shows the contour lines of the water height. Both figures show that the waves spread uniformly and symmetrically, with a radial symmetry away from the center of the dam. Fig. 13 shows plots of the water height along the x-axis obtained using the limiters $MC-2$ and $MC-1.5$ (left) and the limiters $MC-2$ and MinMod (right); results obtained using the $MC-\theta$ limiters are almost identical and are in great agreement with their corresponding ones appearing in [1]; results obtained using the MinMod limiter are less satisfactory.

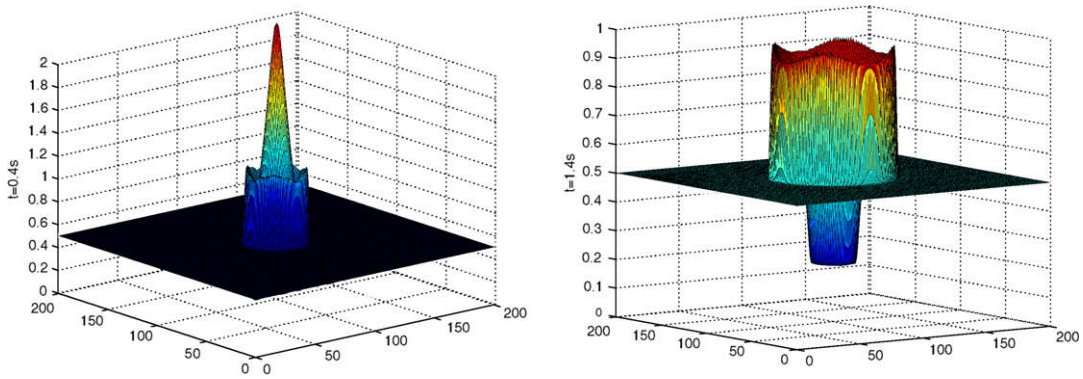

Fig. 14. Toro's reference problem: Water height at times t =0.4 s (left) and t =1.4 s (right).

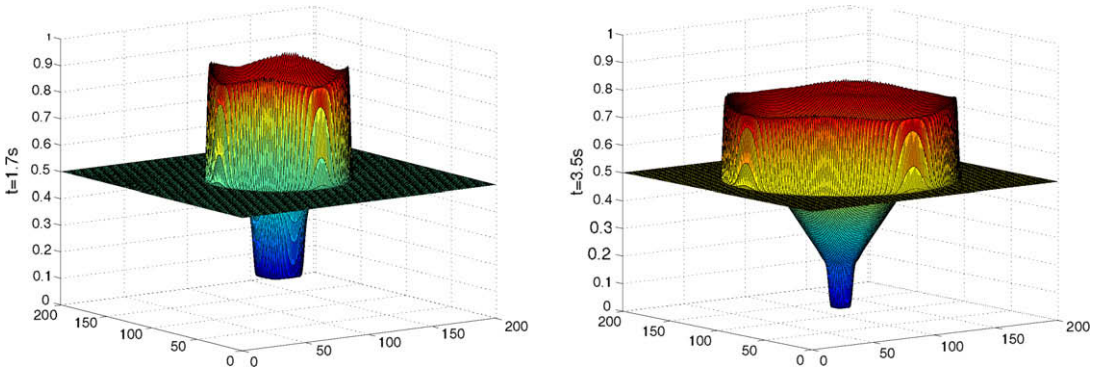

Fig. 15. Toro's reference problem: Water height at times t =1.7 s (left) and t =3.5 s (right).

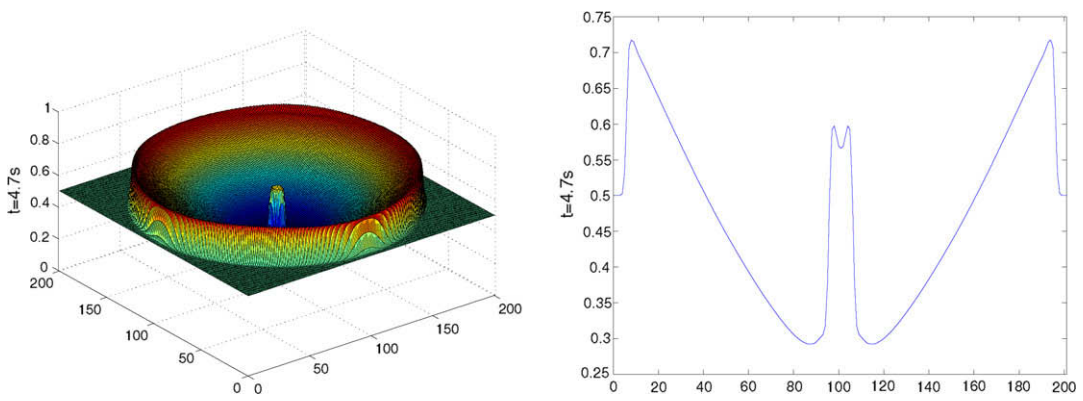

Fig. 16. Toro's reference problem: Water height at time t =4.7 s (left) and a plot of the water height along the line $y = 20$ (right).

4.5. Toro's reference problem

For our final experiment we consider Toro's circular dam-break problem [26] as presented in [12]. The initial conditions for this problem consist of two states: Inside a circular dam of radius 2.5 in the center of the square $[0, 40]^2$ the initial data is $[h, hu, hv] = [2.5, 0, 0]$, while elsewhere in the square the initial data is $[h, hu, hv] = [0.5, 0, 0]$. The computational domain is discretized using 200^2 gridpoints, and the solution is computed using the $MC - (\theta = 2)$ limiter.

Fig. 14 shows the water height at time $t = 0.4$ s (left) and at time $t = 1.4$ s. The water profile shows a circular shock propagating outward radially and an inward propagating rarefaction wave that is about to reach the center of the dam. By the time $t = 1.4$ s the circular rarefaction wave has reached the center of the dam and has reflected producing a water fall in the center of the dam. As discussed in [26], this phenomena is very hard to capture numerically. Fig. 15 shows the water

height at time $t = 1.7$ (left) and time $t = 3.5$. The circular shock has propagated further outwards and the reflected inner circular rarefaction has overexpanded the flow and produced a secondary circular shock propagating towards the center. Fig. 16(left) shows the water height at time $t = 4.7$ s; we see that the secondary shock has already reached the center and has reflected from the center and is now propagating outwards. Fig. 16(right) shows a plot of the water height at the final time $t = 4.7$ s along the line $y = 20$ where we can clearly see two shocks propagating outward.

The results presented in Figs. 14–16 are in good agreement with the corresponding ones presented in [26,11,12].

5. Conclusion

In this paper we have developed one and two-dimensional, non-oscillatory, second-order accurate, unstaggered central scheme for solving systems of hyperbolic equations. The proposed method is an adaptation of the one-dimensional central scheme of Nessyahu and Tadmor, and evolves the numerical solution on a single grid but implicitly uses ghost cells to avoid the time-consuming resolution of the Riemann problems at the cell interfaces. The resulting scheme is a one-parameter method (in one dimension) that computes the numerical solution in two steps. Furthermore, the fact that the numerical scheme does not require any characteristic field decomposition, will significantly reduce computing times as compared with methods based on exact or approximate Riemann-problem solvers. The proposed scheme is second-order accurate both in space and time thanks to piecewise linear interpolants and temporal quadrature rules of order two. As is well known (for central schemes), one should consider several choices of limiters for a given problem. Van Leer's $MC - \theta$ limiter usually leads to good results. For the numerical experiments we considered in this paper, we observed that the value $\theta = 2$ leads to good results with an excellent capture of discontinuities, while the results obtained using the MinMod limiter are less satisfactory.

The numerical method presented in this paper is particularly interesting when solving shallow water problems with variable bottom topography since the updated solution after each time-step is given on the same unique grid where the solution at the previous time, and the bottom topography function, were defined. Therefore the treatment of the source term is immediate and no additional staggering of any function/numerical solution is necessary.

We have solved some SWE problems using both the UCS method and the original multidimensional extensions of the Nessyahu–Tadmor central scheme; the numerical results we obtained using both schemes compare very well to one another and are in very good agreement with corresponding results appearing in the literature, and thus confirm the efficiency and potential of the method.

References

[1] F. Alcrudo, P. Garcia-Navarro, A high resolution Godunov-type scheme in finite volumes for the 2D shallow water equations, Int. J. Numer. Meth. Fluids 16 (1993) 489–505.
[2] P. Arminjon, M.C. Viallon, Généralisation du schéma de Nessyahu–Tadmor pour une équation hyperbolique à deux dimensions d'espace, C.R. Acad. Sci. Paris, t.320, Serie I, 1995, pp. 85–88.
[3] P. Arminjon, D. Stanescu, M.C. Viallon, A two-dimensional finite volume extension of the Lax–Friedrichs and Nessyahu–Tadmor schemes for compressible flows, in: M. Hafez, K. Oshima (Eds.), Proc. 6th. Int. Symp. on Comp. Fluid Dynamics, IV, 1995, pp. 7–14.
[4] P. Arminjon, M.C. Viallon, A. Madrane, A finite volume extension of the Lax–Friedrichs and Nessyahu–Tadmor schemes for conservation laws on unstructured grids, Int. J. Comp. Fluid Dyn. 9 (1) (1997) 1–22.
[5] P. Arminjon, M.C. Viallon, Convergence of a finite volume extension of the Nessyahu–Tadmor scheme on unstructured grids for a two-dimensional linear hyperbolic equation, SIAM J. Num. Anal. 36 (3) (1999) 738–771.
[6] P. Arminjon, R. Touma, Central finite volume methods with constrained transport divergence treatment for ideal MHD, J. Comp. Phys. 204 (2005) 737–759.
[7] N. Botta, R. Klein, S. Langenberg, S. Lützenkirchen, Well balanced finite volume methods for nearly hydrostatic flows, J. Comp. Phys. 196 (2) (2004) 539–565.
[8] F. Bouchut, Nonlinear Stability of Finite Volume Methods for Hyperbolic Conservation Laws and Well-Balanced Schemes for Sources, Birkhäuser Verlag, 2004.
[9] J.U. Brackbill, D.C. Barnes, The effect of nonzero $\nabla\cdot\mathbf{B}$ on the numerical solution of the magnetohydrodynamic equations, J. Comp. Phys. 35 (1980) 426.
[10] M. Castro, J.M. Gallardo, C. Parés, High order finite volume schemes based on reconstruction of states for solving hyperbolic systems with nonconservative products. Applications to shallow-water systems, Math. Comp. 75 (2006) 1103–1134.
[11] A.I. Delis, Th. Katsaounis, Relaxation schemes for the shallow water equations, Int. J. Numer. Meth. Fluids 41 (2003) 695–719.
[12] A.I. Delis, Th. Katsaounis, Numerical solution of the two-dimensional shallow water equations by the application of relaxation methods, Appl. Math. Mod. 29 (2005) 754–783.
[13] T. Gallouët, J.M. Hérard, N. Seguin, Some approximate Godunov schemes to compute shallow water equations with topography, Comp. Fluids 32 (2003) 479–513.
[14] D. George, Finite Volume Methods and Adaptive Refinement for Tsunami Propagation and Inundation, Ph.D. Thesis, University of Washington, 2006.
[15] L. Gosse, A well-balanced flux vector splitting scheme designed for hyperbolic systems of conservation laws with source terms, Comp. Math. App. 39 (2000) 135–159.
[16] J.M. Greenberg, A.Y. LeRoux, A well-balanced scheme for numerical processing of source terms in hyperbolic equations, SIAM J. Numer. Anal. 3 (1996) 1–16.
[17] G.-S. Jiang, D. Levy, C.-T. Lin, S. Osher, E. Tadmor, High-resolution non-oscillatory central schemes with non-staggered grids for hyperbolic conservation laws, SIAM J. Numer. Anal. 35 (1998) 2147–2168.
[18] G. Jiang, E. Tadmor, Non-oscillatory central schemes for multidimensional hyperbolic conservation laws, Siam J. Sci. Comp. 19 (1998) 1892–1917.
[19] A. Kurganov, L. Levy, Central upwind schemes for the St. Venant system, Math. Mod. Numer. Anal. 36 (2002) 397–425.
[20] R. Liska, B. Wendroff, 2D shallow water equations by composite schemes, Int. J. Num. Meth. Fluids 30 (1999) 461–479.
[21] H. Nessyahu, E. Tadmor, Non-oscillatory central differencing for hyperbolic conservation laws, J. Comp. Phys. 87 (2) (1990) 408–463.
[22] S. Noelle, Y. Xing, C.-W. Shu, High order well-balanced finite volume WENO schemes for shallow water equation with moving water, J. Comp. Phys. 226 (2007) 29–58.
[23] S. Noelle, N. Pankratz, G. Puppo, J. Natvig, Well-balanced finite volume schemes of arbitrary order of accuracy for shallow water flows, J. Comp. Phys. 213 (2006) 474–499.

[24] G. Strang, On construction and comparison of difference schemes, SIAM J. Numer. Anal. (1968) 506–517.
[25] P.K. Sweby, High resolution schemes using flux limiters for hyperbolic conservation laws, Siam J. Num. Anal. 21 (1984) 995–1011.
[26] E.F. Toro, Shock-Capturing Methods for Free-Surface Shallow Flows, Wiley, United Kingdom, 2001.
[27] R. Touma, P. Arminjon, Central finite volume schemes with CTCS magnetic field divergence treatment for 2- and 3-D ideal MHD, J. Comp. Phys. 212 (2006) 617–636.
[28] R. Touma, Central unstaggered schemes for one dimensional Shallow water equations, in: Proc. Third Int. Conf. Num. App. Math., ICNAAM 2007, Corfu Greece, September 2007.
[29] B. van Leer, Towards the ultimate conservative difference scheme V. A second-order sequel to Godunov's method, J. Comp. Phys. 32 (1979) 101–136.